SPEKTRUM AKADEMIKA

Volume. 1, Nomor. 1, Mei-Oktober 2026

SYNTHESIS AND EVALUATION OF $NI_{1-x}MN_xFE_2O_4$ FERRITE AS A POTENTIAL RADAR ABSORBING MATERIAL

Yolanda Ferliana Putri[1]*, M. Sulthon Nurharmansyah[2], Muthia Noraina[3]

[1,2,3] Indonesian Defense University, Indonesia

Email: yolandaferlianaputri@gmail.com[1], Sulthonp30@gmail.com[2], muthianoraina7@gmail.com[3]

ABSTRACT

The rapid advancement of modern military and surveillance technology has intensified the need for effective Radar Absorbing Materials (RAM) capable of minimizing electromagnetic wave reflection and reducing radar cross-section (RCS). Spinel ferrites, particularly NiFe2O4 based materials, have attracted considerable attention due to their tunable magnetic and dielectric properties through cation substitution. This study aims to investigate the effect of Mn^{2+} substitution on the structural and magnetic properties of $Ni_{1-x}Mn_xFe_2O_4$ ferrites and to evaluate their potential as radar absorbing materials. $Ni_{1-x}Mn_xFe_2O_4$ ferrites with Mn substitution levels of x = 0.1, 0.3, 0.7, and 0.9 were synthesized using the sol-gel auto-combustion method with stearic acid as a complexing agent. The synthesized powders were characterized in terms of yield efficiency, magnetic response using semi-quantitative magnetic attraction testing, and structural bonding analysis using Fourier Transform Infrared (FTIR) spectroscopy. The synthesis yielded efficiencies ranging from 61.43% to 97.46%, with the highest yield observed at x = 0.1 and the lowest at x = 0.3. Magnetic attraction measurements revealed ferromagnetic behavior in all samples, with magnetic attraction percentages between 77.34% and 94.86%, reaching a maximum at x = 0.9. FTIR spectra confirmed the presence of characteristic metal-oxygen vibrations at tetrahedral and octahedral sites, indicating successful formation of stable spinel structure. Mn substitution was found to influence cation distribution and magnetic interactions within the lattice. The results demonstrate that Mn-doped NiFe2O4 ferrites exhibit tunable structural and magnetic properties, supporting their potential application as radar absorbing materials for defense-related technologies.

Keywords: *Magnetic properties, Mn substitution, Radar Absorbing Materials, Sol-gel, Spinel structure*

INTRODUCTION

Recently, research on spinel ferrite nanoparticles has attracted significant attention due to their distinctive magnetic, electrical, dielectric, and optical properties, which are highly relevant to electromagnetic and defense-related applications. Spinel ferrites are classified as soft magnetic materials with the general formula MFe_2O_4, where M represents divalent metal ions such as Mn, Mg, Zn, Ni, Co, and Cu (Rafiq *et al*., 2020). Among these materials, nickel ferrite ($NiFe_2O_4$) has been extensively studied owing to its favorable characteristics, including low melting temperature, high specific heating capacity, moderate magnetic saturation, and thermal stability. The

ferrimagnetic behavior of $NiFe_2O_4$ originates from antiparallel coupling between Fe^{3+} ions at tetrahedral (A) sites and Ni^{2+}–Fe^{3+} ions at octahedral (B) sites, making it suitable for microwave and electromagnetic wave absorption applications (Khamzina *et al*., 2024).

The physical and magnetic properties of nickel ferrite are strongly influenced by cation substitution, particularly through doping with transition metal ions such as Mn^{2+}. In the $Ni_{1-x}Mn_xFe_2O_4$ system, Mn^{2+} ions partially replace Ni^{2+} ions within the spinel lattice, predominantly occupying octahedral sites, thereby modifying cation distribution and magnetic interactions (Sasikumar *et al*., 2021). This substitution is known to enhance saturation magnetization, increase magnetic permeability, and reduce the optical bandgap, leading to improved electromagnetic wave absorption. Consequently, Mn-doped nickel ferrite has emerged as a promising candidate for Radar Absorbing Material (RAM) applications, particularly in stealth technology aimed at reducing the radar cross-section (RCS) of military platforms (Sharifi *et al*., 2020). Consequently, Mn-doped nickel ferrite has emerged as a promising candidate for Radar Absorbing Material (RAM) applications, particularly in stealth technology aimed at reducing radar cross-section (RCS) of military platforms.

Materials that have the potential to function as radar absorbing materials (RAM) require high magnetic loss, tunable dielectric properties, and efficient interaction with incident electromagnetic waves. In this context, $Ni_{1-x}Mn_xFe_2O_4$ ferrites are considered promising candidates due to their ferrimagnetic behavior, controllable cation distribution, and ability to absorb electromagnetic energy over a broad frequency range.

Several studies have reported that $NiFe_2O_4$ ferrite exhibits good chemical stability, moderate magnetic properties, and potential microwave absorption performance, making it suitable for RAM applications (Emek *et al*., 2025). The magnetic loss mechanism in $NiFe_2O_4$ is mainly associated with natural resonance and domain wall resonance, while its dielectric behavior is influenced by electron hopping between Fe^{2+} and Fe^{3+} ions (Karim & Gul, 2025). To further enhance its electromagnetic properties, partial substitution with transition metal ions such as Mn^{2+} has been widely investigated (Ni *et al*., 2020). Mn substitution is known to modify cation distribution within the spinel structure, influence lattice parameters, and alter magnetic interactions, which may improve magnetic loss and impedance matching characteristics (Karim & Gul, 2025).

However, previous studies on Mn-doped $NiFe_2O_4$ have generally explored only limited substitution levels and narrow composition ranges (Rafie *et al*., 2025). Most investigations focused primarily on crystallinity, particle size, and saturation magnetization without comprehensive evaluation of microwave absorption performance (Nezafat *et al*., 2025). Furthermore, the relationship between Mn concentration, physical properties, magnetic behavior, and radar absorption performance has not been systematically discussed. As a result, composition-dependent optimization of $Ni_{1-x}Mn_xFe_2O_4$ for RAM applications remains insufficiently understood.

Therefore, this study aims to systematically investigate $Ni_{1-x}Mn_xFe_2O_4$ with a broader Mn substitution range to evaluate the relationship between composition, physical properties, magnetic response, and its potential performance as a radar absorbing material. By analyzing these interrelated properties, this research seeks to provide a clearer understanding of how Mn substitution influences electromagnetic wave absorption behavior.

The novelty of this study lies in the systematic investigation of $Ni_{1-x}Mn_xFe_2O_4$ ferrites with a wide range of Mn concentrations (x = 0,1, 0,3, 0,7, and 0,9), synthesized using the sol–gel auto-combustion method. By varying Mn content, this study evaluates how cation distribution and spinel structure influence magnetic behavior and electromagnetic absorption, providing a detailed assessment of their potential as efficient RAM. The sol–gel auto-combustion approach ensures uniform particle size, high crystallinity, and controlled morphology, which are critical for maximizing microwave absorption and improving material performance in stealth applications.

METHOD

Materials

The materials used in this study included nickel(II) nitrate hexahydrate ($Ni(NO_3)_2{\cdot}6H_2O$), manganese(II) nitrate tetrahydrate ($Mn(NO_3)_2{\cdot}4H_2O$), iron(III) chloride hexahydrate ($FeCl_3{\cdot}6H_2O$), stearic acid ($C_{18}H_{36}O_2$) as a complexing agent, and distilled water.

Synthesis Procedure

$Ni_{1-x}Mn_xFe_2O_4$ ferrite powders were synthesized using the sol–gel auto-combustion method. Stoichiometric amounts of metal precursors corresponding to x = 0,1, 0,3, 0,7, and 0,9 were mixed with stearic acid at 70 °C. Distilled water was added to initiate sol formation through hydrolysis and condensation reactions (Pinto *et al*., 2024). The resulting sol was continuously stirred using a glass overhead stirrer to avoid redox contamination.

The sol was dried at approximately 100 °C to obtain a dry gel, which was subsequently subjected to auto-combustion at 400 °C. The combustion reaction occurred spontaneously due to the interaction between organic fuel and metal ions, producing ferrite powder along with gaseous byproducts (Ahmed *et al*., 2024).

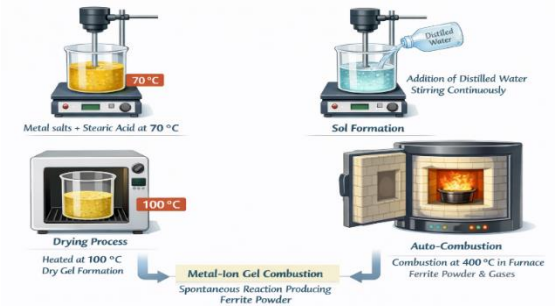

Figure 1. Synthesis procedure of $Ni_{1-x}Mn_xFe_2O_4$ ferrite powders

Characterization Methods

Physical observation was conducted to evaluate color, texture, and homogeneity of the synthesized powders. Yield was calculated by comparing theoretical and actual mass values. Magnetic attraction was evaluated using a semi-quantitative method by measuring the mass of powder attracted by a permanent magnet.

Physical Observation

The synthesized $Ni_{1-x}Mn_xFe_2O_4$ ferrite powders were initially characterized through macroscopic physical observation. The color of each sample was recorded to identify possible compositional variations and phase formation resulting from different Mn substitution levels (x = 0,1, 0,3, 0,7, and 0,9). Texture and particle appearance were examined visually to assess powder fineness, degree of agglomeration, and uniformity. Homogeneity was evaluated qualitatively by observing the consistency of color and the absence of visible unreacted precursors or secondary phases. All observations were performed under identical lighting conditions to ensure consistency (Baydin *et al*., 2022).

Yield Determination

The synthesis yield was determined to evaluate the efficiency of the sol–gel auto-combustion process. The theoretical mass of $Ni_{1-x}Mn_xFe_2O_4$ was calculated based on the stoichiometric molar ratios of the starting metal precursors used during synthesis. After the auto-combustion process and cooling to room temperature, the resulting ferrite powder was carefully collected and weighed using an analytical balance with ±0.1 mg precision. This analysis provides information regarding material loss during gel drying, combustion, and post-synthesis handling (Çelik *et al*., 2024).

Magnetic Attraction Test (Semi-Quantitative Method)

The magnetic properties of the synthesized powders were evaluated using a simple magnetic attraction test. A fixed mass of ferrite powder (e.g., 0.5 g) was placed in a non-magnetic container. A permanent magnet was positioned at a fixed distance (about 1–2 cm) above the

powder for 30 seconds. After that, the magnet was removed carefully, and the powder attached to the magnet was collected and weighed using an analytical balance. The mass of the attracted powder was used as an indicator of magnetic strength. All samples were tested under the same distance and time conditions to ensure fair comparison. This method does not provide detailed magnetic parameters such as saturation magnetization or coercivity, but it is useful as a preliminary comparison before further testing using instruments like Vibrating Sample Magnetometry (VSM) (Martin *et al*., 2022).

RESULTS AND DISCUSSION

Synthesis of $Ni_{1-x}Mn_xFe_2O_4$

The synthesis of ferrite using metal precursors $Ni(NO_3)_2{\cdot}6H_2O$, $Mn(NO_3)_2{\cdot}4H_2O$, and $FeCl_3{\cdot}6H_2O$ was carried out using the sol–gel auto-combustion method. The compositional variations (x) applied in the ferrite synthesis were 0,1, 0,3, 0,7, and 0,9. All metal precursors were mixed with a complexing agent (stearic acid) at a temperature of 70 °C. The reaction involved is expressed as follows:

$$(1\text{-}x)Ni(NO_3)_2.6H_2O_{(s)} + xMn(NO_3)_2.4H_2O_{(s)} + 2FeCl_3.6H_2O_{(s)} + C_{18}H_{36}O_{2(s)} \rightarrow$$
$$\rightarrow (1\text{-}x)Ni(C_{18}H_{36}O_2)_{2(s)} + xMn(C_{18}H_{36}O_2)_2(s) + 2Fe(C_{18}H_{36}O_2)_{3(s)}$$

Stearic acid was used as a complexing agent in the synthesis of $Ni_{1-x}Mn_xFe_2O_4$ due to its amphiphilic structure, which provides an ideal balance between hydrocarbon chain length and the binding strength of polar functional groups (Chen *et al*., 2020). The long C18 carbon chain imparts hydrophobic characteristics that support the formation of a two-phase system (water–oil) during the sol process, while the short and polar carboxylate group (–COOH) can strongly interact with Ni^{2+}, Mn^{2+}, and Fe^{3+} ions through coordination bonding or the formation of metal–stearate complex. This structure ensures good steric stability, facilitates precursor homogenization, and controls ferrite particle growth, resulting in fine particle size and uniform morphology (Shi & Peng, 2021).

The use of fatty acids with excessively short chains, such as citric acid (C8), tends to exhibit hydrophilic behavior, allowing them to dissolve completely in the liquid medium without forming the two-phase (water–oil) system required in sol–gel processes to control particle growth (Lopes *et al*., 2019). Under such conditions, the reaction occurs in a single homogeneous liquid phase. The absence of steric hindrance from long hydrocarbon chains allows uncontrolled growth of metal oxide particles, leading to agglomeration or the formation of large crystals with non-uniform size distribution (Xu *et al*., 2023). In contrast, fatty acids with excessively long carbon chains, such as lignoceric acid, are highly hydrophobic. Lignoceric acid, with a C24 carbon chain, generates excessive steric hindrance that inhibits effective homogenization of metal precursors and reduces the efficiency of complex formation (Wang *et al*., 2024). Consequently, the gelation process becomes slower, particle formation is less uniform, and the resulting particles tend to be larger with a broad size distribution (Zhang *et al*., 2024).

The mixture of metal precursor solutions and stearic acid was then added with distilled water to initiate the sol–gel formation process. The addition of distilled water served to dissolve the metal salts uniformly and create favorable conditions for hydrolysis and condensation, which are two critical stages in gel formation (Bokov *et al*., 2021). During this stage, metal ions from the precursors react with hydroxyl groups formed in the solution, producing a three-dimensional network that binds metal particles within a homogeneous matrix (Sharma *et al*., 2018). Stirring was carried out using an overhead stirrer with a glass agitator to prevent redox reactions and avoid contamination in the form of hematite (Fe_2O_3) (Li *et al*., 2019). After the stirring process was completed and a stable sol was obtained, the subsequent step was drying in an oven to remove residual moisture. This process was conducted gradually at approximately 100 °C until all remaining water had evaporated, resulting in a dry gel ready for the combustion stage. Drying not only removes water but also strengthens the gel network (Adams, 2018). The dried gel was

then subjected to auto-combustion at 400 °C using a furnace. This stage constitutes the core of the sol–gel auto-combustion method, where spontaneous combustion occurs due to the interaction between the organic compound (stearic acid) and metal ions trapped within the gel matrix (Khamidy *et al*., 2025). The chemical reaction occurring during the auto-combustion process is exothermic and can be represented as follows:

$$(1\text{-}x)Ni(C_{18}H_{36}O_2)_{2\,(s)} + xMn(C_{18}H_{36}O_2)_{2\,(s)} + 2Fe(C_{18}H_{36}O_2)_{3\,(s)}$$

$$\rightarrow Ni_{1\text{-}x}Mn_xFe_2O_{4\,(s)} + CO_{2\,(g)} + H_2O_{\,(l)} + NO_{x\,(g)}$$

Physical Property Testing of $Ni_{1-x}Mn_xFe_2O_4$

Figure 2. Results of Ni1-xMnxFe2O4 samples (0,1; 0,3; 0,7; and 0,9)

Based on observations of the physical properties of $Ni_{1-x}Mn_xFe_2O_4$ materials with varying concentrations of Mn^{2+} ion substitution (x = 0,1, 0,3, 0,7, and 0,9), it was found that all samples exhibited a dominant grayish-black color, with differences in color intensity, texture, and powder consistency. The appearance of a grayish-black color in all samples indicates the successful formation of ferrite compounds. The ferrite powders at x = 0,1, 0,3, and 0,7 tended to show a grayish-black color, whereas the sample at x = 0,9 exhibited a darker gray-black appearance

Observations of the samples with x = 0,1, 0,7, and 0,9 revealed a finer powder texture with a stable dry consistency. This behavior is attributed to good crystallinity and relatively uniform particle size. In contrast, the sample with x = 0,3 showed agglomeration in the ferrite powder texture. This agglomeration phenomenon occurs due to Van der Waals interactions induced by residual H_2O molecules that did not completely evaporate or detach during the synthesis and drying processes. The presence of these H_2O molecules creates intermolecular bridges that enhance attractive forces between particles, causing fine particles to adhere to one another and form small agglomerates (Zhou *et al*., 2020).

Based on these physical observations, the synthesis yield was calculated to evaluate the efficiency of $Ni_{1-x}Mn_xFe_2O_4$ formation for each compositional variation. The following is shown in Table 1. is the yield of ferrite metal synthesis results.

Tabel 1. Yield of $Ni_{1-x}Mn_xFe_2O_4$ Synthesis Results

x	Theoretical Mass (g)	Actual Mass (g)	%Yield
0,1	2,885	2,812	97,46
0,3	2,885	1,772	61,43
0,7	2,885	2,801	97,09
0,9	2,885	2,548	88,33

The yield of ferrite synthesis results in all variations of samples produced a percentage of more than 50%, this indicates that ferrite synthesis was running efficiently. The highest yield was obtained at variation x = 0,1, amounting to 97,46%, while the lowest at x = 0,3 was 61,43%. The decrease in yield was caused by mass loss due to the spillage of part of the sample during the calcination process at high temperatures.

$Ni_{1-x}Mn_xFe_2O_4$ Magnetic Attraction Test

The magnetic attraction test was conducted to qualitatively evaluate the magnetic properties of $Ni_{1-x}Mn_xFe_2O_4$ samples with varying Mn substitution levels (x = 0,1, 0,3, 0,7, and 0,9). This test aimed to observe the response of the ferrite powders to an external magnetic field as an initial indication of ferromagnetic behavior. Through visual analysis of the powder distribution and movement when brought close to a magnet, the degree of magnetic attraction for each composition can be observed. Differences in powder accumulation on the side nearest to the magnet indicate variations in magnetic interaction strength due to the effect of Mn ion substitution within the formed spinel structure, based on Figure 2.

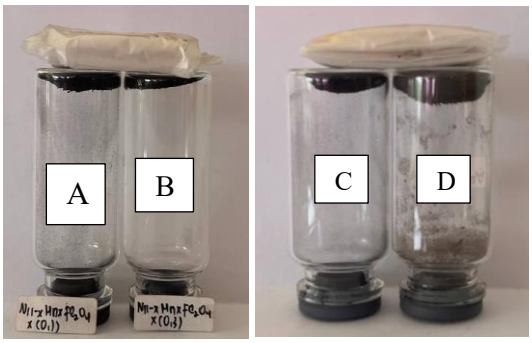

Figure 3. $Ni_{1-x}Mn_xFe_2O_4$ Magnetic Attraction Test Results A. x(0,1), B. x(0,3), C. x(0,7), and D. x(0,9)

Tabel 2. $Ni_{1-x}Mn_xFe_2O_4$ Magnetic Attraction Test

x	Weighted Mass (g)	Mass is Attracted to a Magnet (g)	% Magnet Attraction
0,1	0,254	0,218	85,82
0,3	0,253	0,229	90,51
0,7	0,256	0,198	77,34
0,9	0,253	0,240	94,86

Based on Table 2, the results of the semi-quantitative magnetic attraction test show that all samples have ferromagnetic properties with a magnetic attraction percentage value above 70%. The highest value was obtained at variation x = 0,9, amounting to 94,86%, while the lowest value was at x = 0,7, amounting to 77,34%. The increase in magnetic attraction at higher x variations shows that the addition of Mn^{2+} ions to a certain extent can strengthen the total magnetic moment in the spinel ferrite structure. This happens because Mn^{2+} has a greater magnetic moment than Ni^{2+} (Dippong *et al*., 2022). At variation x = 0,7, a significant decrease in magnetic attraction can be seen. This can be caused by the uneven distribution of Mn^{2+} ions in the spinel lattice, thereby disrupting the regularity of the internal magnetic field and reducing the exchange interactions between the spinels. Apart from that, the possibility of particle agglomeration can also reduce magnetic properties due to the formation of magnetic domains that are not perfectly aligned (Blachowicz *et al*., 2022).

The synthesis of $Ni_{1-x}Mn_xFe_2O_4$ ferrite requires an initial characterization stage to ensure the formation of a metal oxide network as the foundation of its magnetic and electromagnetic properties (Ashiq, 2023). FTIR analysis is employed at the preliminary stage because this technique can rapidly, specifically, and efficiently identify the presence of metal–oxygen bonds (Gong *et al*., 2024). FTIR provides information regarding the formation of characteristic M–O vibrations in the spinel structure without requiring complex sample preparation. However, FTIR data cannot explain the crystal structure in detail nor the electromagnetic wave absorption

performance. FTIR only functions as an initial indicator that the synthesis has produced a metal oxide framework with potential to be developed as a magnetic material.

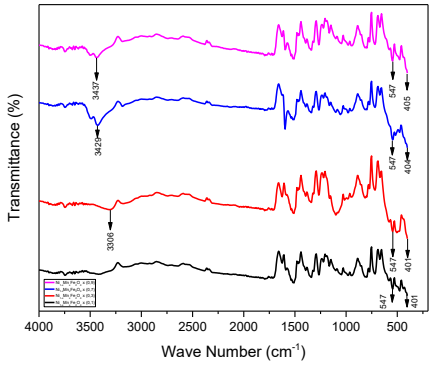

Figure 4. Infrared Spectrum of $Ni_{1-x}Mn_xFe_2O_4$ Sample

Based on Figure 3, the FTIR spectrum shows a broad absorption band in the range of 3300–3450 cm^{-1}, representing the stretching vibration of –OH groups originating from adsorbed water or surface hydroxyl groups. The spectrum also displays a band around 1600 cm^{-1} corresponding to the bending vibration of H–O–H. The low wavenumber region of 600–400 cm^{-1} exhibits a strong band around 547 cm^{-1} associated with the metal–oxygen stretching vibration at the tetrahedral site, as well as bands at approximately 467, 444, 405, and 401 cm^{-1} related to metal–oxygen vibrations at the octahedral site. The presence of these two characteristic bands indicates that metal cations are distributed in two coordination sites typical of the spinel structure. These data suggest that the ferrite formation reaction has occurred and produced stable M–O bonds FTIR cannot determine crystallite size, phase purity, magnetic parameters, or the reflection loss value of the material. FTIR cannot measure the ability of the material to absorb electromagnetic waves. FTIR only demonstrates that the structural prerequisite, namely the formation of metal–oxygen bonds, has been achieved. The presence of these bonds provides initial potential that the material may exhibit characteristic ferrite magnetic properties. This potential still requires confirmation through XRD for phase analysis, VSM for magnetic parameters, SEM for morphology, and VNA for evaluation of Radar Absorbing Material performance.

The synthesis of $Ni_{1-x}Mn_xFe_2O_4$ theoretically produces a spinel structure with two types of cation coordination environments. FTIR analysis is conducted to ensure that the metal–oxygen bonds forming the primary spinel framework have been established. FTIR is selected as an initial characterization technique because it can detect characteristic M–O vibrations that form the basis of ferrite magnetic behavior. FTIR is not used to prove performance as a Radar Absorbing Material, but rather to confirm that the required fundamental chemical structure has been formed. The FTIR spectral data show a broad absorption band in the range of 3300–3450 cm^{-1} with peaks at approximately 3437, 3429, and 3306 cm^{-1}. These bands correspond to the –OH stretching vibration originating from adsorbed water or residual surface hydroxyl groups from the synthesis process. A band around 1600 cm^{-1} corresponds to the H–O–H bending vibration, indicating the presence of weakly bound water molecules. The presence of these bands indicates that residual hydroxyl groups remain in the sample but do not interfere with the identification of the main ferrite bands in the low wavenumber region.

The 600–400 cm^{-1} region shows a strong band around 547 cm^{-1} corresponding to the metal–oxygen stretching vibration at the tetrahedral (A-site). The data also show bands at approximately 467, 444, 405, and 401 cm^{-1} corresponding to metal–oxygen vibrations at the octahedral (B-site). The appearance of these two main bands serves as a characteristic indicator of the cubic spinel structure. The relatively sharper intensity of the ~547 cm^{-1} band indicates the dominance of M–O vibration at the tetrahedral site. Slight variations in wavenumber position within the 400–500 cm^{-1} range indicate the influence of Mn substitution on bond length and force

constants within the crystal lattice. These shifts are consistent with the difference in ionic radius between Ni^{2+} and Mn^{2+}, which affects cation distribution. The FTIR data demonstrate that the formation of the M–O–M network has occurred and produced a stable metal oxide framework. These data only confirm the successful formation of the fundamental chemical structure of ferrite. FTIR cannot provide information regarding phase purity, crystallite size, magnetic parameters, or electromagnetic wave absorption capability. Discussion of the material's potential as a radar absorbing material must be supported by further characterization using XRD, VSM, SEM, and VNA. In this context, FTIR serves as preliminary evidence that the material possesses the structural foundation necessary for the emergence of characteristic ferrite magnetic properties.

CONCLUSION

$Ni_{1-x}Mn_xFe_2O_4$ (x = 0,1, 0,3, 0,7, and 0,9) was successfully synthesized using the sol–gel auto-combustion method with stearic acid as a complexing agent. The synthesis yields were effective, ranging from 61,43% to 97,46%, with the highest yield observed at x = 0,1. All samples exhibited ferromagnetic behavior, with magnetic attraction percentages between 77,34% and 94,86%, indicating that the magnetic properties can be tuned through Mn substitution. FTIR analysis confirmed the formation of metal–oxygen (M–O) bonds at both tetrahedral and octahedral sites, demonstrating the successful formation of a stable spinel framework.

SUGGESTION FOR FUTURE RESEARCH

Further research is recommended to conduct comprehensive structural, magnetic, and electromagnetic characterization using advanced techniques such as XRD, SEM, VSM, and vector network analyzer (VNA) measurements to evaluate reflection loss and impedance matching behavior. Investigating the correlation between Mn concentration, microstructure, and microwave absorption performance over a wider frequency range would provide deeper insight into the optimization of this material for RAM applications. In addition, the development of composite systems incorporating polymer matrices or conductive fillers may enhance dielectric–magnetic synergy and improve absorption efficiency for practical stealth and electromagnetic interference shielding applications.

REFERENCES

Adams, D. (2018). Does Drying Affect Gel Networks Gels, 4(2), 32. https://doi.org/10.3390/gels4020032

Ahmed, N., Khalil, Z., Farooq, Z., Khizar-Ul-Haq, N., Shahida, S., Ramiza, N., Ahmad, P., Qadir, K. W., Khan, R., & Zafar, Q. (2024). Structural, Optical, and Magnetic Properties of Pure and Ni-Fe-Codoped Zinc Oxide Nanoparticles Synthesized by a Sol-Gel Autocombustion Method. ACS Omega, 9(1), 137–145. https://doi.org/10.1021/acsomega.3c01727

Ashiq, M. G. B. (2023). Structural, dielectric, morphological and magnetic properties of cobalt-substituted nickel spinel ferrites (CoxNi1-xFe2O4) nanoparticles. Applied Nanoscience, 13(6), 4541–4554. https://doi.org/10.1007/s13204-022-02750-w

Baydin, A., Hernandez, F. G. G., Rodriguez-Vega, M., Okazaki, A. K., Tay, F., Noe, G. T., Katayama, I., Takeda, J., Nojiri, H., Rappl, P. H. O., Abramof, E., Fiete, G. A., & Kono, J. (2022). Magnetic Control of Soft Chiral Phonons in PbTe. Physical Review Letters, 128(7), 075901. https://doi.org/10.1103/PhysRevLett.128.075901

Blachowicz, T., Grzybowski, J., & Ehrmann, A. (2022). Influence of agglomerations on magnetic properties of polymer matrices filled with magnetic nanoparticles. Materials Today: Proceedings, 67, 792–796. https://doi.org/10.1016/j.matpr.2022.07.362

Bokov, D., Turki Jalil, A., Chupradit, S., Suksatan, W., Javed Ansari, M., Shewael, I. H., Valiev, G. H., & Kianfar, E. (2021). Nanomaterial by Sol-Gel Method: Synthesis and Application. Advances in Materials Science and Engineering, 2021(1). https://doi.org/10.1155/2021/5102014

Çelik, Ş., Tutar, H., Gönülal, E., & Er, H. (2024). Prediction of fresh herbage yield using data mining techniques with limited plant quality parameters. Scientific Reports, 14(1), 21396. https://doi.org/10.1038/s41598-024-72746-9

Chen, Q., Shi, Y., Chen, G., & Cai, M. (2020). Enhanced mechanical and hydrophobic properties of composite cassava starch films with stearic acid modified MCC (microcrystalline cellulose)/NCC (nanocellulose) as strength agent. International Journal of Biological Macromolecules, 142, 846–854. https://doi.org/10.1016/j.ijbiomac.2019.10.024

Dippong, T., Levei, E. A., Deac, I. G., Petean, I., & Cadar, O. (2022). Dependence of Structural, Morphological and Magnetic Properties of Manganese Ferrite on Ni-Mn Substitution. International Journal of Molecular Sciences, 23(6), 3097. https://doi.org/10.3390/ijms23063097

Emek, M., Şahin, E., Ibrahim, J., & Kartal, M. (2025). Electromagnetic Shielding Performance of Ta-Doped NiFe2O4 Composites Reinforced with Chopped Strands for 7–18 GHz Applications. Nanomaterials, 15(20), 1580. https://doi.org/10.3390/nano15201580

Gong, Y., Chen, X., & Wu, W. (2024). Application of fourier transform infrared (FTIR) spectroscopy in sample preparation: Material characterization and mechanism investigation. Advances in Sample Preparation, 11, 100122. https://doi.org/10.1016/j.sampre.2024.100122

Karim, A., & Gul, I. H. (2025). Study of structural, dielectric, and magnetic properties of nickel doped strontium hexaferrite nanoparticles for microwave absorption application. Materials Research Express, 12(9), 095008. https://doi.org/10.1088/2053-1591/ae0275

Khamidy, N. I., Kamal, M. N., Mufakhir, F. R., Nurfani, E., Triyadi, D., Satria, R., & Nisa, F. K. (2025). Simple preparation of metal alloys by sol–gel autocombustion method. Materials Letters, 382, 137894. https://doi.org/10.1016/j.matlet.2024.137894

Khamzina, Zh., Kudaibergenova, R., & Baibazarova, E. (2024). SYNTHESIS AND CHARACTERIZATION OF NiFe2O4 SPINEL NANOPARTICLES. Chemical Journal of Kazakhstan, (4), 87–94. https://doi.org/10.51580/2024-4.2710-1185.51

Li, Z., Chanéac, C., Berger, G., Delaunay, S., Graff, A., & Lefèvre, G. (2019). Mechanism and kinetics of magnetite oxidation under hydrothermal conditions. RSC Advances, 9(58), 33633–33642. https://doi.org/10.1039/C9RA03234G

Lopes, J. H., Bueno, O. M. V. M., Mazali, I. O., & Bertran, C. A. (2019). Investigation of citric acid-assisted sol-gel synthesis coupled to the self-propagating combustion method for preparing bioactive glass with high structural homogeneity. Materials Science and Engineering: C, 97, 669–678. https://doi.org/10.1016/j.msec.2018.12.022

Martin, L. M. A., Sheng, J., Zimba, P. V., Zhu, L., Fadare, O. O., Haley, C., Wang, M., Phillips, T. D., Conkle, J., & Xu, W. (2022). Testing an Iron Oxide Nanoparticle-Based Method for Magnetic Separation of Nanoplastics and Microplastics from Water. Nanomaterials, 12(14), 2348. https://doi.org/10.3390/nano12142348

Nezafat, Z., Jafari, G., Javanshir, S., & Peymanfar, R. (2025). MXene-based metal oxide/metal composites for microwave absorption and shielding: recent advances and future perspectives. Advanced Composites and Hybrid Materials, 8(6), 447. https://doi.org/10.1007/s42114-025-01535-3

Ni, Q., Sun, L., Cao, E., Hao, W., Zhang, Y., & Ju, L. (2020). Enhanced magnetic and dielectric properties of NiFe2O4 ferrite ceramics co-substituted by (Li1+, Zn2+ and La3+). Ceramics International, 46(7), 9722–9728. https://doi.org/10.1016/j.ceramint.2019.12.240

Pinto, O. M., Toledo, R. P., Barros, H. E. da S., Gonçalves, R. A., Nunes, R. S., Joshi, N., & Berengue, O. M. (2024). Advances and Challenges in WO3 Nanostructures' Synthesis. Processes, 12(11), 2605. https://doi.org/10.3390/pr12112605

Rafie, S. F., Abu-Zahra, N., & Sillanpää, M. (2025). A comprehensive review of spinel ferrites and their magnetic composites as highly efficient adsorbents of rare earth elements. Emerging Contaminants, 11(1), 100429. https://doi.org/10.1016/j.emcon.2024.100429

Rafiq, M. A., Javed, A., Rasul, M. N., Khan, M. A., & Hussain, A. (2020). Understanding the structural, electronic, magnetic and optical properties of spinel MFe2O4 (M = Mn, Co, Ni) ferrites. Ceramics International, 46(4), 4976–4983. https://doi.org/10.1016/j.ceramint.2019.10.237

Sasikumar, K., Bharathikannan, R., Sujithkumar, G., Raja, S., Arputhavalli, G. J., Vidhya, M., Marnadu, R., & Suresh, R. (2021). Structural, Optical, and Magnetic Properties of Mn-Doped Nickel Ferrite (Ni1-xMnxFe2O4) Thin Films Deposited by Jet Nebulizer Spray Pyrolysis Technique. Journal of Superconductivity and Novel Magnetism, 34(8), 2189–2198. https://doi.org/10.1007/s10948-021-05948-1

Sharifi, S., Yazdani, A., & Rahimi, K. (2020). Incremental substitution of Ni with Mn in NiFe2O4 to largely enhance its supercapacitance properties. Scientific Reports, 10(1), 10916. https://doi.org/10.1038/s41598-020-67802-z

Sharma, M., Pathak, M., & Kapoor, P. N. (2018). The Sol-Gel Method: Pathway to Ultrapure and Homogeneous Mixed Metal Oxide Nanoparticles. Asian Journal of Chemistry, 30(7), 1405–1412. https://doi.org/10.14233/ajchem.2018.20845

Shi, S.-C., & Peng, Y.-Q. (2021). Hydrophobicity and Macroscale Tribology Behavior of Stearic Acid/Hydroxypropyl Methylcellulose Dual-Layer Composite. Materials, 14(24), 7707. https://doi.org/10.3390/ma14247707

Wang, B., Zheng, H., Yang, Y., Bian, X., Ma, C., Zhang, Y., Liu, X., Wang, Y., Zhang, G., Sun, S., & Zhang, N. (2024). Effect of different chain-length fatty acids on the retrogradation properties of rice starch. Food Chemistry, 461, 140796. https://doi.org/10.1016/j.foodchem.2024.140796

Xu, H., Tian, H., Deng, J., Zhuo, Q., Cui, J., Wang, J., Yin, Y., & Yu, P. (2023). Review of influence of steric effect on aggregation behavior of fine particles. Minerals Engineering, 203, 108304. https://doi.org/10.1016/j.mineng.2023.108304

Zhang, H., Du, S., Wang, Y., & Xue, F. (2024). Prevention of Crystal Agglomeration: Mechanisms, Factors, and Impact of Additives. Crystals, 14(8), 676. https://doi.org/10.3390/cryst14080676

Zhou, J., Lin, S., Zeng, H., Liu, J., Li, B., Xu, Y., Zhao, X., & Chen, G. (2020). Dynamic intermolecular interactions through hydrogen bonding of water promote heat conduction in hydrogels. Materials Horizons, 7(11), 2936–2943. https://doi.org/10.1039/D0MH00735H